Liquid Crystals
Publication details, including instructions for authors and subscription information:
http://www.informaworld.com/smpp/title~content=t713926090

Image analysis of shear-induced textures in liquid-crystalline polymers

J. T. Gleeson[ab]; R. G. Larson[a]; D. W. Mead[ac]; G. Kiss[d]; P. E. Cladis[a]
[a] AT&T Bell Laboratories, Murray Hill, New Jersey, U.S.A. [b] Department of Physics, Kent State University, Kent, Ohio, U.S.A. [c] Shell Development Corporation, Houston, Texas, U.S.A. [d] Bell Communications Research, New Jersey, U.S.A.

To cite this Article Gleeson, J. T. , Larson, R. G. , Mead, D. W. , Kiss, G. and Cladis, P. E.(1992) 'Image analysis of shear-induced textures in liquid-crystalline polymers', Liquid Crystals, 11: 3, 341 — 364
To link to this Article: DOI: 10.1080/02678299208028994
URL: http://dx.doi.org/10.1080/02678299208028994

LIQUID CRYSTALS, 1992, VOL. 11, NO. 3, 341–364

Image analysis of shear-induced textures in liquid-crystalline polymers

by J. T. GLEESON†‡, R. G. LARSON*†, D. W. MEAD†§, G. KISS¶ and P. E. CLADIS†

† AT&T Bell Laboratories, Murray Hill, New Jersey 07974, U.S.A.
‡ Department of Physics, Kent State University, Kent, Ohio 44242, U.S.A.
§ Shell Development Corporation, P.O. Box 1380, Houston, Texas 77251, U.S.A.
¶ Bell Communications Research, Red Bank, New Jersey 07701, U.S.A.

(*Received 25 February 1991; accepted 1 May 1991*)

Textures of several liquid-crystalline solutions of poly(benzylglutamate) and a solution of hydroxypropylcellulose were videorecorded during and after shear and the images were Fourier transformed. We find for all the solutions that bands perpendicular to the flow direction form after cessation of prolonged shearing if the Deborah number De exceeds a critical value $De_C \approx 0{\cdot}1$. Here $De = \tau\dot{\gamma}_0$, where $\dot{\gamma}_0$ is the shear rate and τ is the characteristic molecular relaxation time. The bands are characterized by an initially broad spectrum of wavelengths; for the poly(benzylglutamate) solutions this spectrum narrows and shifts towards longer wavelengths as time progresses after cessation of shear, leading to an increase in the characteristic band spacing $b(t)$ with time t. The dependences of the band spacing on the shear rate $\dot{\gamma}_0$ and on the solution viscosity η in poly(benzylglutamate) are very weak, but the time to form bands after shearing ceases is roughly inversely proportional to $\dot{\gamma}_0$. Our results suggest that both molecular elasticity and texture elasticity influence band formation, and that the texture elasticity is not described by small gradient (Frank) theory.

1. Introduction

Unlike small-molecule liquid crystals, whose technological applications usually demand the achievement of a state of uniform orientation of the director field, liquid-crystalline polymers in their existing and most probable future applications will most likely be imperfectly aligned, or *textured* materials. Indeed, the attainment of a state of uniform orientation in these polymers is difficult [1–4] and this uniformity is easily destroyed when the material flows [3] as it does when it is being shaped into a useful product. Thus it would seem essential to gain some understanding of the textures that persist in static samples of liquid-crystalline polymers, as well as of the texture evolution that occurs during, and after, flow [5, 6].

There are a variety of peculiar rheological and optical properties of liquid-crystalline polymers that are thought to be influenced or controlled by the dynamics of texture evolution in these materials. These include the slowly damped oscillations in stress and dichroism seen during shear flows when the rate of shear or its direction is suddenly changed [7, 8], and the scaling of stresses [7–9] and other rheological

* Author for correspondence.

responses such as recoverable strain [10] with time multiplied by shear rate, rather than with time itself. We would like to understand how textures influence rheological properties, such as those just mentioned, and how the textures that persist after cessation of flow can influence the orientation and hence the physical properties of the final product material. Unfortunately, despite their evident importance, as yet there has been no experimental quantification of complex textures, and hence no way to relate textures quantitatively to rheological or mechanical properties.

Recent theoretical work has focused on the characteristic domain size, a, in units of length, as the most important characteristic of the texture [11–13]. The quantity a can be thought of as a correlation length over which the orientation within a textured specimen is roughly uniform. If the texture is produced in a static sample by disclination lines that permeate the sample, then a^{-2} is the total length of the disclination lines per unit volume of the sample. A region of roughly uniform orientation is often called a domain. If the material is subjected to steady flow or a strong external field, there is also a direction of preferred alignment induced by the flow or external field, with short-range deviations from that alignment because of trapped disclinations, defects, or other imperfections. Thus, in addition to the domain size a, the degree of domain alignment is potentially another important characteristic of the texture. Rudimentary phenomenological theories of texture development have recently been proposed that make predictions of rheological properties such as those mentioned previously [14, 15].

Although these theoretical descriptions of the texture seem to be useful in rationalizing some of the observed rheological characteristics of liquid-crystalline polymers, we again point out that there have been few, if any, attempts to quantify the domain spacing a or other characteristics of the texture in experiments with well-controlled flow fields. In this article, we introduce image analysis of video-recorded textures of liquid-crystalline polymers as a direct method of texture characterization. In particular, here we quantify black and white video images using the fast Fourier transform (FFT).

Although a light or X-ray scattering experiment also provides a Fourier transform of a real-space image, direct image analysis has at least two potential advantages that make it useful as well. The first is that the method of applying the FFTs via computer software to a videorecorded image can be tailored to amplify particular features of the image. As detailed later, amplification of a certain feature (namely bands) is achieved in our application by applying FFTs to individual horizontal lines of the video image, and then averaging over many such lines. In a scattering experiment, the equivalent amplification could only be achieved by introducing specialized optical elements, which might be difficult to configure and align. A second advantage is that we retain the real-space images, which we can compare to the corresponding FFTs. A difficulty with a typical scattering method is that, while it is a superb means of quantifying structure, it is usually not a reliable means of even qualitatively identifying the shapes of the structures that produce the scattering. To take a simple example, it may not be possible using scattering alone to be sure that a suspension of spheres of various sizes is not actually a suspension of ellipsoids. (Once the elementary shapes are known from some other means such as microscopy, scattering is an excellent means of quantifying the sizes of the objects and their spacing.) The structures that produce the FFTs we obtain from the videorecorded images can, on the other hand, be examined visually at will. Video analysis, then, combines some of the quantitative strengths of scattering with the qualitative strengths of microscopy.

Perhaps the most interesting, and certainly the most studied, texture that appears in liquid-crystalline polymers as a result of shearing is the transverse banded texture that has been observed to form shortly after cessation of shearing [16–29]. The bands, which are distinct under crossed polaroids, are oriented perpendicular to the direction of the previous flow and in the plane parallel to the shearing surfaces. Thus the bands are parallel to the y direction, where x is the flow direction and z is the gap direction in the shearing cell. The bands consist of alternating dark and light regions, along with variations in coloration. Such bands have been observed in thermotropic nematics [17–21], lyotropic nematics [21, 29], and in cholesterics such as hydroxypropylcellulose [21–28] (HPC) and poly(γ-benzylglutamate) [16] (PBG) solutions. The bands form either almost immediately after shearing stops or may take more than a minute to form, depending on the shear rate and the duration of the shearing. After shearing at a high rate, the bands are usually rather straight when they first form, but become wavy and finally disappear altogether as time progresses [27].

In HPC and poly(n-hexylisocyanate) solutions, the bands were not observed at all if the shear rate or the duration of the shearing was too low [24, 25, 29]. The gaps used in the experiments ranged from 3 μm to 500 μm. The widths of the bands that formed ranged from 0·5 μm to 10 μm, depending mainly on the material, and little or not at all on the gap. Marrucci *et al.* [25] reported by visual inspection of HPC solutions that the shear strains required to form bands became less as the gap was increased, while Ernst and Navard [24] reported that there was no effect of the gap on the critical condition for band formation. The discrepancy between these workers may be due in part to the subjectiveness of the observations. In marginal cases, the bands become very weak in appearance and a report of their existence or non-existence is based on the judgement of the observer [25]. Fincher found using a diffraction technique that the band width b in HPC was also independent of time after shearing ceased, and was independent of the shear rate $\dot{\gamma}_0$ and gap h [28]; Ernst and Navard [24] concur that the band width is independent of $\dot{\gamma}_0$ and h for HPC, but for a thermotropic cellulosic polymer, Navard and Zachariades have stated that b decreases with increasing $\dot{\gamma}_0$ [19]. A similar decrease in b with increasing $\dot{\gamma}_0$ was reported by Zachariades *et al.* for a thermotropic liquid-crystalline polymer [18]. It has also been reported that the time t_b required after cessation of shear for bands to form decreases as $\dot{\gamma}_0$ increases [16, 24, 29]. According to Kiss and Porter, [16] for PBG solutions, 'with increasing rate of prior shear the [banded] texture forms more rapidly, with better definition and thinner striations, and also degenerates more quickly'. These observations are consistent with ours, as reported later.

The optical contrast that defines the bands is evidently provided by a spatial modulation in the molecular orientation. Specifically, it has been found that the director varies in a serpentine manner between the angles $+\alpha$ and $-\alpha$ to the x (flow) direction as we move from band to band along the x direction [16, 19, 22, 27]. Between crossed polaroids with one polarizer's transmission axis parallel to the flow direction, the dark bands are produced when the director passes through an angle of zero degrees with respect to the x direction, and the light bands occur when the director is at an angle of $+\alpha$ or $-\alpha$. The angle α has been variously reported to be 15–24° [22] and 45° [16, 19, 27]. Thus following cessation of shearing, some source of elastic energy drives the director into a zig–zag pattern with respect to the flow direction.

Finally, we note that bands perpendicular to the previous flow direction have also been seen in drawn fibres [18, 27], with a band spacing about 10 times finer than that found after shearing flows [18].

2. Experimental

2.1. *The flow cell*

The flow cell used for our texture studies is depicted in figure 1. The lower stainless steel plate of this device contains an annular trough the bottom of which is composed of glass. The sample is loaded into this trough. The lower plate is mounted on a bearing and its edge has geared teeth so that it can be driven by a belt and a stepper motor; the rotation speed can range from 2×10^{-4} to $2\,\text{rev}\,\text{s}^{-1}$. The upper non-rotating plate is mounted on a shaft that is coaxial with the bearing on which the lower plate is mounted. The shaft can be translated along its axis by a micrometer, thus allowing the gap between the upper and lower plates to be adjusted over a range from 50 μm to 4000 μm with a precision of about 50 μm. For a typical gap of 150 μm, the range of available motor speeds allows the attainment of a shear rate range of 0·4 to $4000\,\text{s}^{-1}$. The stationary upper plate is made of stainless steel except for a small 0·25 in diameter

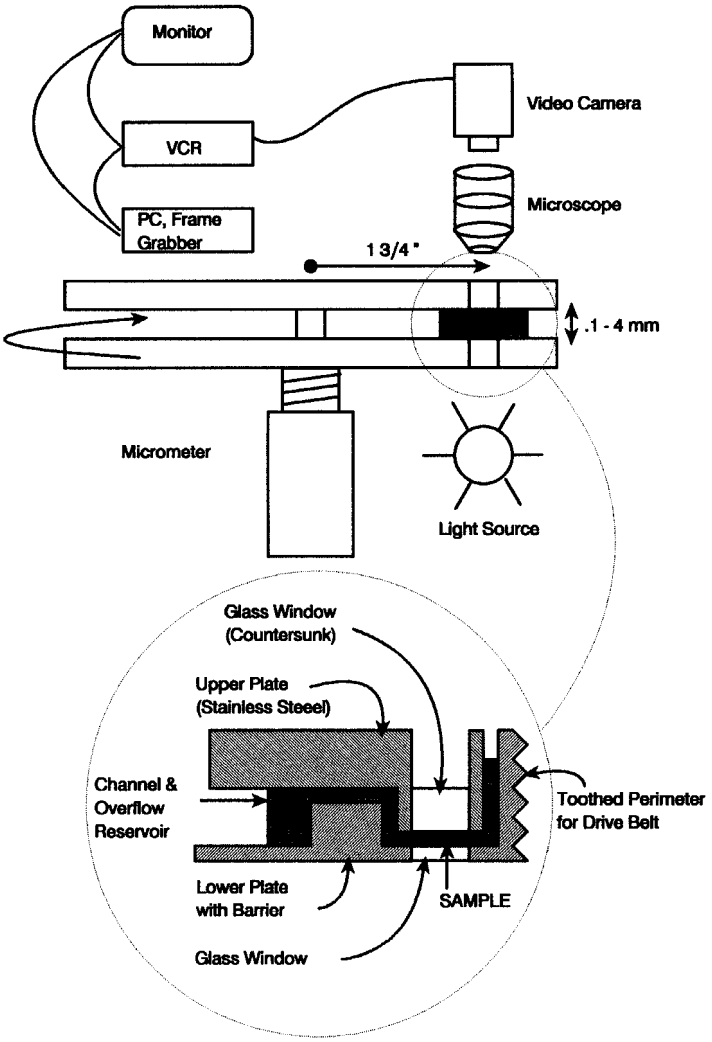

Figure 1. Schematic drawing of the shearing-flow microscopy cell.

glass window, through which the sample residing between the two plates can be viewed. The outer 0·31 in of the upper plate, in which the window is situated, is thicker than the rest of the plate; this thick lip can be lowered into the trough of the lower plate, and be brought into contact with the sample by dialing down the micrometer. The lip of the upper plate is slightly narrower than the width of the trough so that air bubbles and excess fluid can be driven out of the glass bottom trough on the lower plate. A stainless steel overflow trough on the inner portion of the lower plate captures the excess fluid that is squeezed out of the glass bottom trough when the gap is decreased, and prevents it from spilling into the bearing. No attempt was made to control the boundary conditions on either the upper or lower plates.

The entire assembly was mounted on the stage of a Nikon Optiphot-pol polarizing microscope, and was situated so that the incident beam of polarized light passed through the annular glass ring on the lower plate and the window of the upper plate. The transmission axis of the incident polarized light was parallel to the flow direction, while the transmission axis of the analyser was perpendicular to the flow direction. A Hitachi VK-C150 camera was mounted on top of the microscope, permitting the video recording of colour images of the texture at the rate of 30 frames s^{-1} with a Panasonic AG-6020 time-lapse videorecorder. The PBG solutions were all videotaped through a $\times 10$ magnification objective lens. All experiments were carried out at room temperature, about 23°C.

2.2. *Materials*

Four lyotropic liquid-crystalline polymer samples were examined in detail; all contained PBG in the solvent metacresol, and all contained a concentration of polymer at or near the minimum required to form a fully liquid-crystalline phase; the molecular weights and concentrations of PBG are listed in table 1. The sample of intermediate molecular weight, PBG118, was a racemic mixture composed of PBLG with a viscosity average molecular weight M_v of 86 000 and its enantiomorph PBDG with an M_v of 150 000. The other samples contained only PBLG in metacresol. The ratios of weight to number average molecular weights of these PBLG materials was about 1·7. The properties of a sample of hydroxypropylcellulose in water, studied by Ernst and Navard [24], is also included in table 1 for future reference.

The shear viscosities η and first normal stress differences N_1 of the four samples as functions of shear rate $\dot{\gamma}$ are plotted in figures 2 (*a*)–(*d*). These were measured at room temperature using a 50 mm diameter 0·04 radian cone and plate fixture on the Rheometrics System 4 rheometer. PBLG solutions generally show three regimes of the first normal stress difference [30, 31], with positive values at low shear rates, negative values at intermediate shear rates, and positive values at high shear rates. PBLG238

Table 1. Properties of PBG and HPC samples.

Sample	Polymer wt.%	Molecular weight M	$\dot{\gamma}_{me}/s^{-1}$	$\dot{\gamma}_b/s^{-1}$
PBLG86	31	86000	>400	≈40
PBG118	21	118000	200	≈5
PBLG186	14	186000	15	≈0·25
PBLG238	12·5	238000	5	<1
HPC60 [24]	60	60000	30	≈2

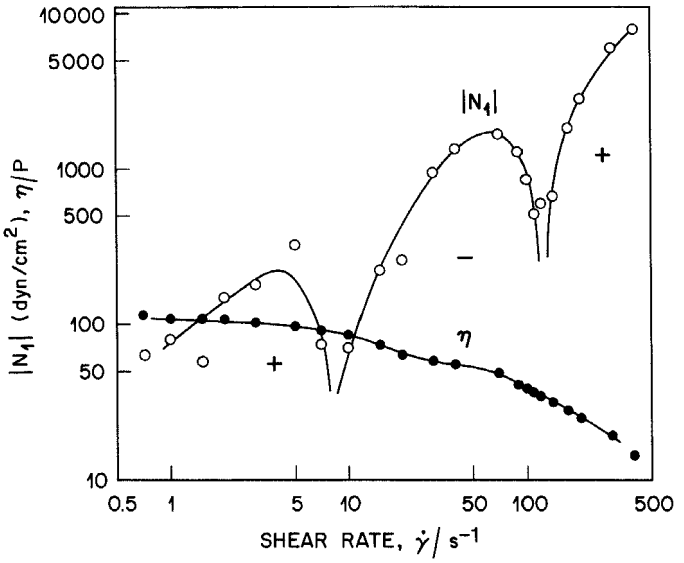

(*a*)

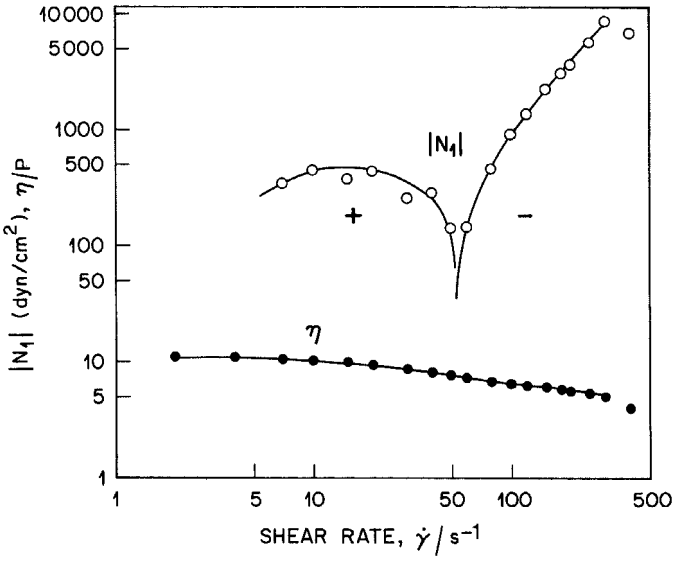

(*b*)

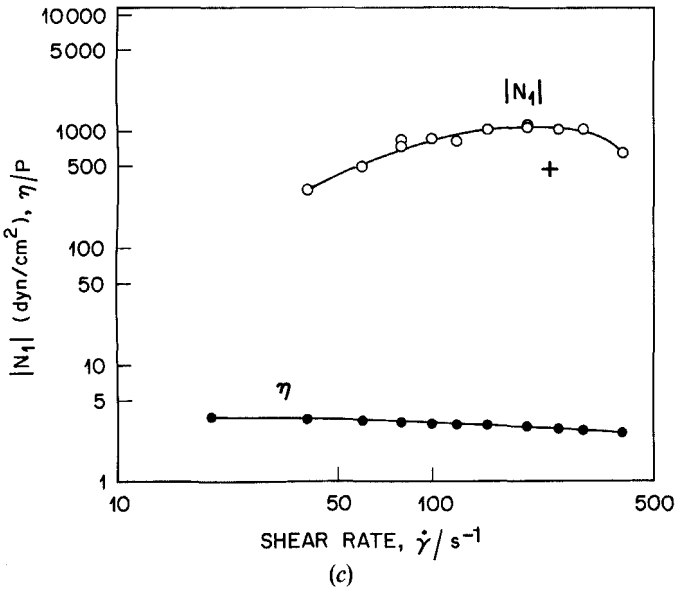

(*c*)

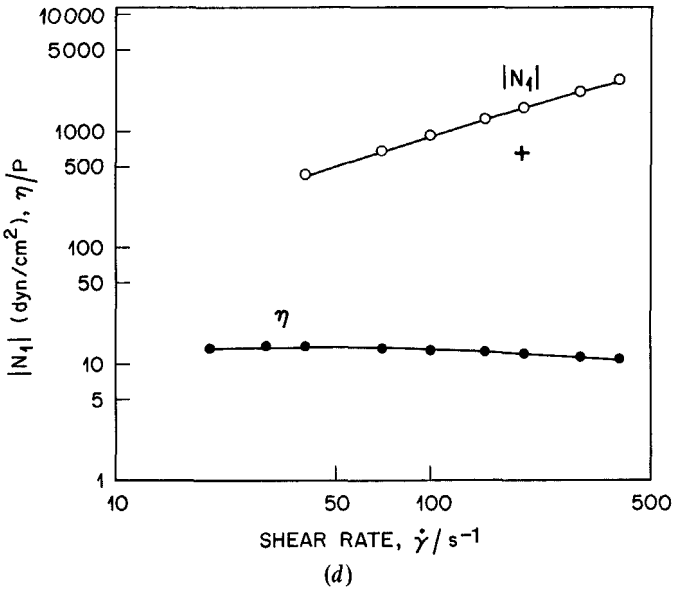

(*d*)

Figure 2. (*a*) Shear viscosity and absolute value of the first normal stress difference versus shear rate for PBLG238 (MW = 238 000). (*b*) Shear viscosity and absolute value of the first normal stress difference versus shear rate for PBLG186 (MW = 186 000). (*c*) Shear viscosity and absolute value of the first normal stress difference versus shear rate for PBG118 (MW = 118 000). (*d*) Shear viscosity and absolute value of the first normal stress difference versus shear rate for PBLG86 (MW = 86 000).

shows all three regimes within the accessible range of shear rates (see figure 2 (*a*)). The molecular relaxation time τ_{mol} decreases rapidly with decreasing molecular weight [32] and this shifts the normal stress regimes to higher shear rates. Thus, for PBLG186, in figure 2 (*b*), only the first two normal stress regimes are accessed at the shear rates available to us; the third regime has been shifted to shear rates too high for our instrument to measure. For PBG118 and PBLG86 (see figures 2 (*c*) and (*d*)) all but the first regime of positive first normal stress difference N_1 lie outside the available range of shear rates. PBG118 does, however, show the first positive maximum in N_1, while for PBLG86, this maximum evidently occurs at a shear rate higher than $400\,s^{-1}$.

Using the molecular theory of Doi [32] it is possible to explain the existence of the three regimes in terms of arrested director tumbling [33, 34]. Tumbling has recently been shown to occur experimentally in a PBG solution [4]. Tumbling is arrested because of molecular elasticity which we define here as the elastic response created by shear-induced distortions of the local (sub-domain) distribution of molecular orientations. We distinguish molecular elasticity from texture elasticity, which we shall have more to say about later. Molecular elasticity is important, for example, when flow changes the degree of small-scale molecular alignment (the scalar order parameter) in a nematic; this produces an elastic response at the molecular level. The presence of a significant level of molecular elasticity is signalled by a maximum in the first normal stress difference as a function of shear rate. From figure 2, we estimate the shear rates $\dot{\gamma}_{me}$ at which N_1 passes through a positive maximum value. The results appear in table 1, along with $\dot{\gamma}_{me}$ for an HPC solution studied by Ernst and Navard. At the shear rate $\dot{\gamma}_{me}$, according to the Doi molecular theory, the Deborah number ($De = \tau_{mol}\dot{\gamma}$) is about 0·5. Here τ_{mol} is the relevant molecular relaxation time, namely $1/6\bar{D}_r$, where $\bar{D}_r$ is the effective molecular rotary diffusivity [32, 33].

The four PBG solutions studied in detail had shear viscosities in the range 4–100 P. One much more viscous solution was investigated less systematically. This was a solution of 54 wt.% HPC (Klucel L) in acetic acid; it has a shear viscosity of 1000–2000 P in the range of shear rates ($1–10\,s^{-1}$) over which it's textures were studied.

3. Results

3.1. *Qualitative visual observations*

Our visual observations of band formation after cessation of steady shearing are qualitatively similar, for the most part, to those of earlier workers. When shearing begins on a sample that had been quiescent for several minutes, a series of stripes typically form; these stripes are irregularly spaced several microns apart, and are parallel to the flow direction. Sometimes before the formation of these stripes, bands perpendicular to the flow can be seen; these eventually disappear, however. We suspect that the perpendicular bands photographed during shear in early studies of Kiss and Porter [16], thought by them to exist at steady state, were actually the same transient features we report here. After cessation of shear, the parallel stripes disappear at a rate that increases with increasing prior shear rate $\dot{\gamma}_0$. Thereafter bands can form that are perpendicular to the previous shearing direction.

At high shear rates, imposition of some 40–80 shearing strain units are required for our solutions to form bands, and these bands appear within seconds after shear ceases. Once formed, the bands in PBG solutions appear to widen as time progresses, and they eventually disintegrate. When the shear rate $\dot{\gamma}_0$ is decreased enough, we find that the strain γ_b that must be applied to obtain bands increases dramatically; we must wait

much longer after shearing ceases, up to several minutes, for bands to appear. For low enough $\dot{\gamma}_0$, even a thousand strain units is insufficient to obtain bands. Figure 3 shows the dependence of γ_b on $\dot{\gamma}_0$ obtained by visual inspection of PBLG186 at three different gaps h. Similar results were obtained by Marrucci *et al.* [25] and by Ernst and Navard [24] for HPC solutions; except that Marrucci *et al.* [25] reported a significant decrease of γ_b with increasing gap at fixed $\dot{\gamma}_0$, while Ernst and Navard found no dependence of γ_b on the gap. Our observations seem to show little gap dependence. If there is any at all, it is opposite to that observed by Marrucci *et al.* However, to the eye, the distinction between the presence and absence of bands is not sharp. At intermediate conditions, the assessment of whether bands are present or not is highly subjective; and this could lead to variations in our estimate of γ_b by as much as a factor of two. The wish to avoid such subjectivity is one reason we turn to image analysis in the next section. Another factor that complicates transient measurements such as those presented in figure 3 is the long memory that liquid-crystalline polymers have of their prior shear history. Thus, in what follows, we restrict our study of band formation to experiments in which shearing is prolonged for at least a thousand strain units, during which time the texture, averaged over the sample, appears to attain a steady state.

In table 1 we record an estimate of the minimum shear rate $\dot{\gamma}_b$ required to form bands after imposition of at least 1400 strain units, for three of our PBG materials. Note that for each of these $\dot{\gamma}_b$ is at least a factor of five less than $\dot{\gamma}_{me}$, the shear rate at which N_1 has a positive maximum. Ernst and Navard [24] found $\dot{\gamma}_b$ to be about a factor of about 15 less than $\dot{\gamma}_{me}$ for an HPC solution; this is also recorded in table 1.

3.2. *Image analysis*

The textures of the liquid-crystalline polymer solutions both during and after shear were viewed through the polarizing microscope and recorded on video tape. On playback, individual frames are digitized at fixed intervals after the shearing stops. The

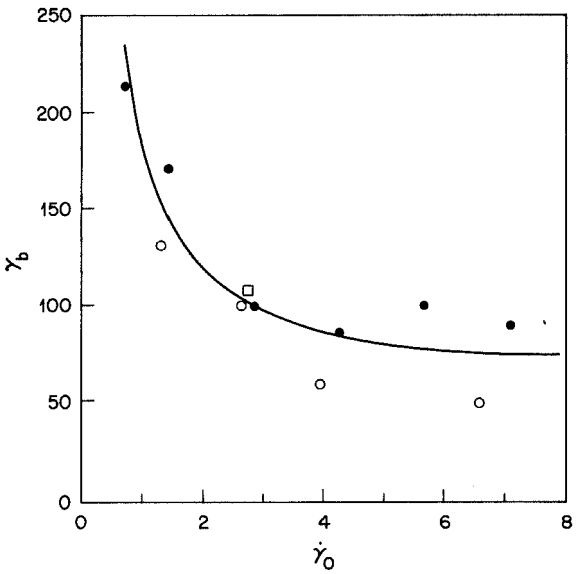

Figure 3. Visual observation of minimum shear strain γ_b required to form bands as a function of shear rate $\dot{\gamma}_0$ for PBLG186 at gaps h of 175 μm (○), 330 μm (●) and 860 μm (□).

frame grabber has a resolution of 512×480 pixels with 256 gray scales. Since the structures we are interested in are almost always spatially incoherent, we can improve the signal by performing the FFT on the individual horizontal (vertical) video lines and then, at each spatial frequency, we can average the resulting Fourier amplitude over all horizontal (vertical) lines. The horizontal video lines are parallel to the x (or flow) direction. Thus, the average of the horizontal FFTs gives a one dimensional FFT that characterizes length scales parallel to flow, such as the widths of transverse bands, while the average of the vertical FFTs characterizes the vertical length scales perpendicular to flow. After cessation of shearing, we find that the averaged horizontal FFT contains significant power at wavelengths comparable to the typical band spacings perceived by the eye. The averaged vertical FFT usually contains much less power at finite wavelengths; this reflects the visual observation that there is little structure parallel to the flow after cessation of shearing.

Figure 4(*a*) shows the texture observed 10 s after the shear was stopped for PBLG186. The shear rate was $10{\cdot}28\,s^{-1}$ and roughly 1500 shear strain units were imposed. The gap between the shearing surfaces was about 175 μm. Figure 4(*b*) is the

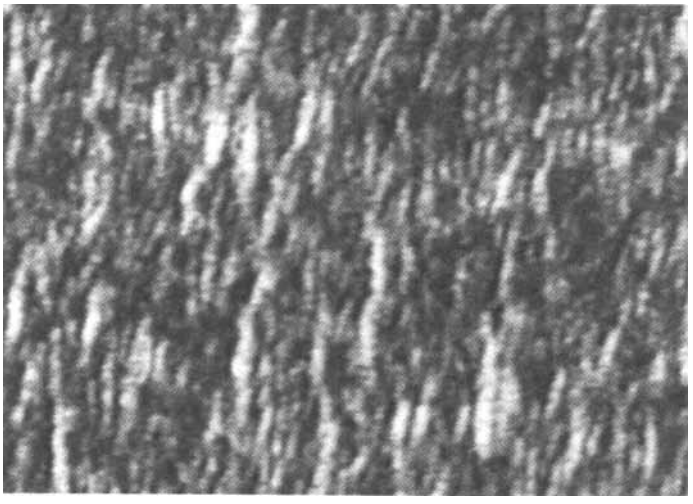

(*a*)

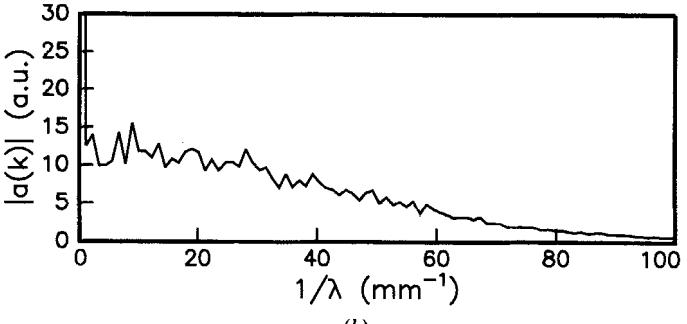

(*b*)

Figure 4. (*a*) Image of texture of PBLG186 observed through crossed polarizers 10 s after shear was stopped. $\dot{\gamma}_0 = 10{\cdot}28\,s^{-1}$, $\gamma_0 = 1460$, $h = 175\,\mu$m. The horizontal width of the image is approximately 890 μm. (*b*) FFT obtained from the image in (*a*).

horizontal spatial fast Fourier transform of this image, obtained as described earlier. The most striking feature is the broad and fairly flat spectrum containing wavelengths ranging from the width of the screen down to around 10 μm. The width of the spectrum shrinks as the texture evolves. The texture and corresponding FFT at 70 s after the shear stopped is shown in figure 5. In figure 6, which superposes the spectra from figures 4 and 5, the general trend to longer wavelengths referred to earlier can be seen to occur in two ways: the Fourier amplitudes at short wavelengths are significantly attenuated while those at in the longer wavelength grow somewhat.

We quantity this behaviour by defining a characteristic wavelength λ^* such that

$$\frac{1}{2} \equiv \frac{\int_0^{2\pi/\lambda^*} a(k)\,dk}{\int_0^{\infty} a(k)\,dk}, \tag{1}$$

where $a(k)$ is the Fourier amplitude at wavenumber k. Thus, half the integral under the spectrum has wavelength greater than λ^*; the other half of the integral is in wavelengths less than λ^*. We denote the characteristic wavelength for horizontal spectra by $\lambda^*_{\parallel}$; $\lambda^*_{\parallel}$

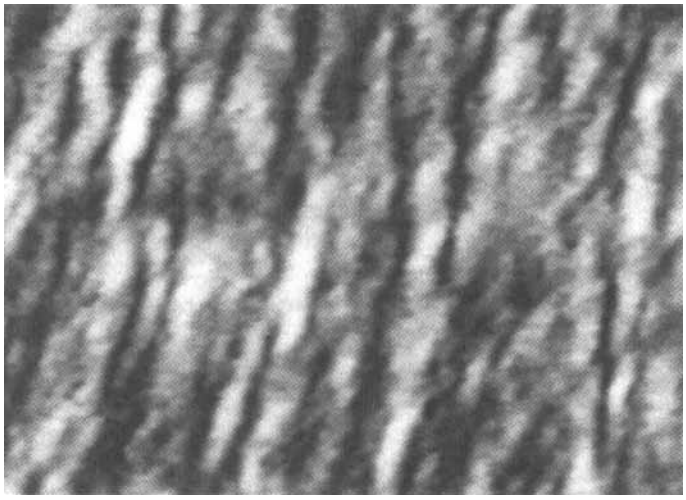

(*a*)

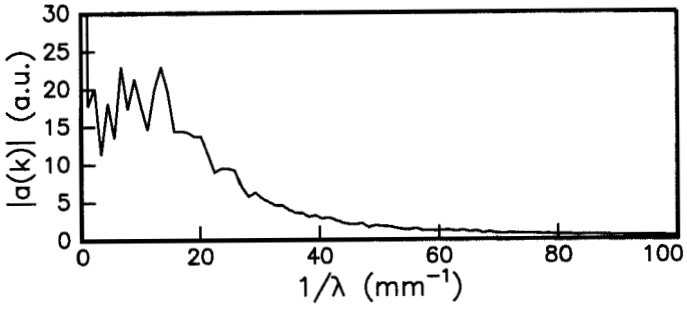

(*b*)

Figure 5. (*a*) Image of texture of PBLG186 70 s after shear was stopped. Same run as previous figure. (*b*) FFT obtained from the image in (*a*).

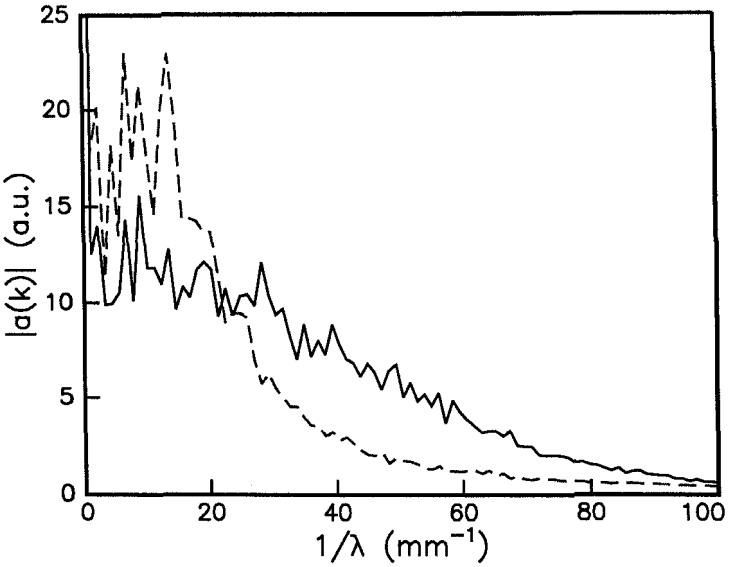

Figure 6. FFTs from figures 4 and 5 superimposed, showing the diminution of power in the short wavelength part of the spectrum at long times after cessation of shear. Here the solid line is for 10 s, and the dashed line for 70 s, after shearing was stopped.

reflects the average length scale parallel to the previous shearing flow. Similarly $\lambda_{\perp}^{*}$ shall denote the characteristic wavelength for vertical spectra. When bands are observed in PBG, $\lambda_{\parallel}^{*}$ generally increases with time, as we shall soon show in detail.

Sometimes, during later stages of the band-coarsening process, a sharp peak in the spectrum temporarily appears and then vanishes after several seconds; figure 7 shows an example. The wavelength of the peak, when it occurs, is usually roughly equal to the gap, h. Although we have seen this sharp peak several times, it does not occur reproducibly, even if the shear rate and gap are the same. We therefore suspect that its occurrence is related to the smallness of the region (around 1×1 mm) in the sample contained within the field of view of the video; perhaps regions this small occasionally have a high degree of spatial coherence not possessed by other regions of the same sample. If this is so, then spectra obtained on larger portions of the material would show this peak only in greatly attenuated form, or not at all.

Figure 8 shows $\lambda_{\parallel}^{*}$ and $\lambda_{\perp}^{*}$ versus time after cessation of shearing for a shear rate $\dot{\gamma}_0 = 5{\cdot}14\,\mathrm{s}^{-1}$ for PBLG186 at a gap of 175 μm. At this shear rate, perpendicular bands were first observed visually at around 20 s after cessation of shearing. At a much higher shear rate, $\dot{\gamma}_0 = 20{\cdot}57\,\mathrm{s}^{-1}$, the bands appear almost instantly after cessation of shearing; $\lambda_{\parallel}^{*}$ and $\lambda_{\perp}^{*}$ for this shear rate are shown in figure 9. Note that for both $\dot{\gamma}_0 = 5{\cdot}14\,\mathrm{s}^{-1}$ and $\dot{\gamma}_0 = 20{\cdot}57\,\mathrm{s}^{-1}$, $\lambda_{\parallel}^{*}(t=0) > \lambda_{\perp}^{*}(t=0)$ and both $\lambda_{\parallel}^{*}$ and $\lambda_{\perp}^{*}$ generally increase with time following cessation of shearing. However, for the higher shear rate, $\lambda_{\perp}^{*}$ increases much faster with time than $\lambda_{\parallel}^{*}$, and quickly crosses over it so that $\lambda_{\perp}^{*} > \lambda_{\parallel}^{*}$. This crossover occurs at roughly the same time that bands perpendicular to the flow direction become clearly visible to the eye. A similar crossover occurs for $\dot{\gamma}_0 = 10{\cdot}28\,\mathrm{s}^{-1}$; the crossover time for $\dot{\gamma}_0 = 10{\cdot}28\,\mathrm{s}^{-1}$ is larger than for $\dot{\gamma}_0 = 20{\cdot}57\,\mathrm{s}^{-1}$, and so is the time for appearance of the bands. Thus, for the higher two shear rates, the crossover of $\lambda_{\perp}^{*}$ and $\lambda_{\parallel}^{*}$ seems to be linked to the formation of the bands. For the two lower shear rates, $\lambda_{\perp}^{*}$ and $\lambda_{\parallel}^{*}$ do not cross; in these cases band formation occurs when $\lambda_{\perp}^{*}$ and $\lambda_{\parallel}^{*}$ first come to their closest

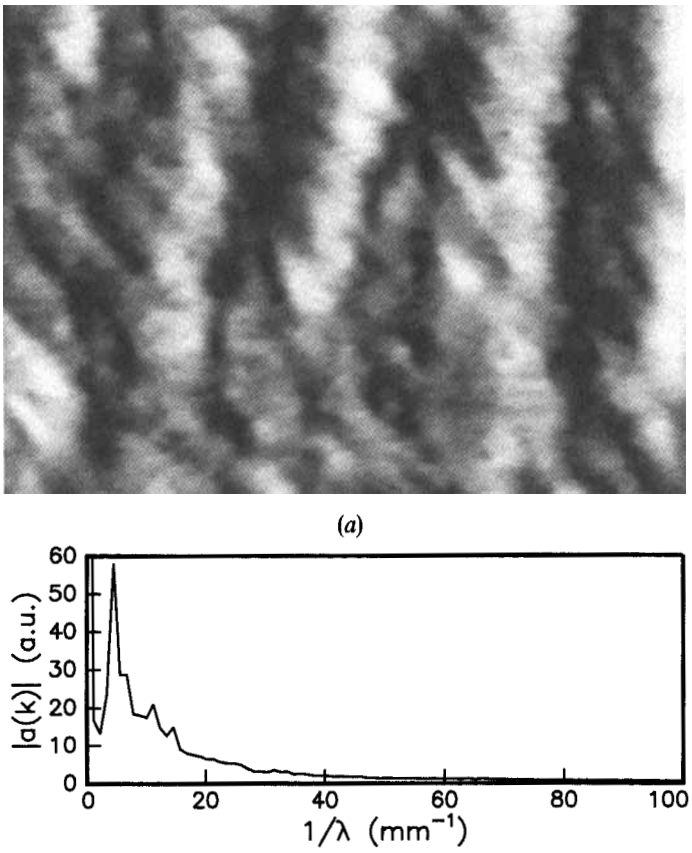

Figure 7. (*a*) Image of texture of PBLG186 observed through crossed polarizers 235 s after shearing was stopped; same run as figures 4 and 5. $\dot{\gamma}_0 = 10{\cdot}28\,s^{-1}$, $\gamma_0 = 1460$, $h = 175\,\mu m$. The horizontal width of the image is about 890 μm. (*b*) FFT obtained from the image in (*a*).

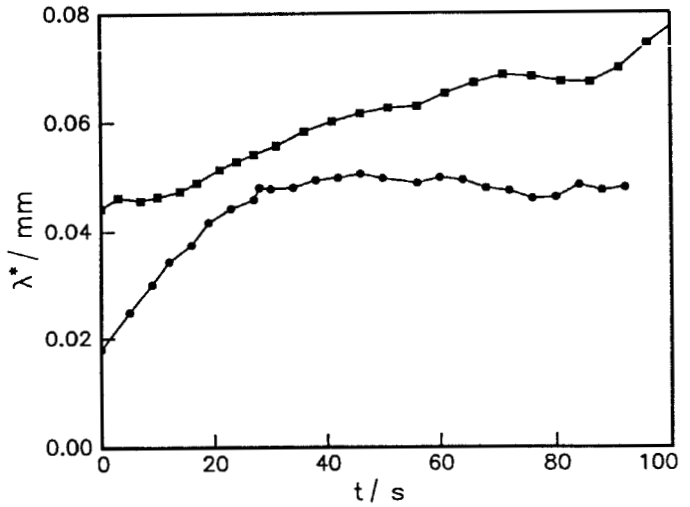

Figure 8. $\lambda_{\parallel}^{*}$ (■) and $\lambda_{\perp}^{*}$ (●) versus time for PBLG186 with $\dot{\gamma}_0 = 5{\cdot}14\,s^{-1}$, $\gamma_0 \approx 1400$, and $h = 175\,\mu m$. The bands can be seen by eye at $t \approx 20$ s.

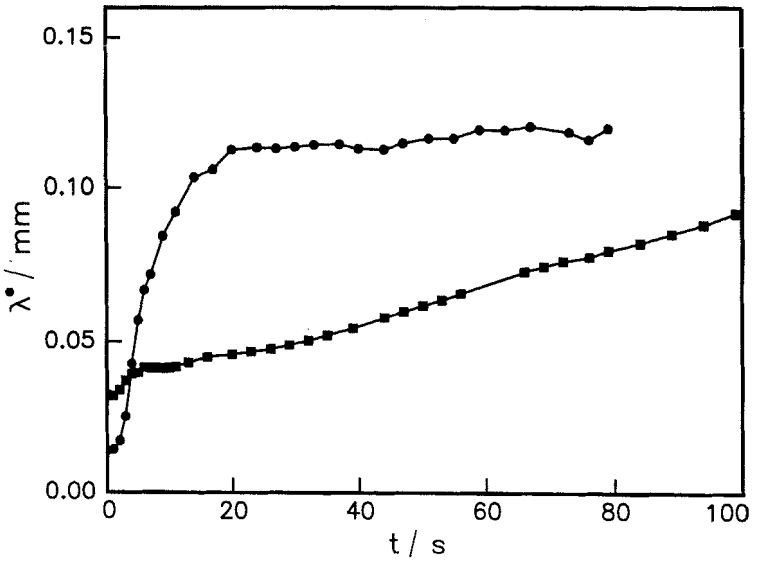

Figure 9. $\lambda_{\parallel}^{*}$ (■) and $\lambda_{\perp}^{*}$ (●) versus time for PBLG186 with $\dot{\gamma}_0 = 20{\cdot}57\,s^{-1}$, $\gamma_0 \approx 1400$, and $h = 175\,\mu m$. The bands can be seen by eye at $t \approx 3\,s$.

Table 2. Characteristic wavelengths during shearing and time to form bands after shearing in PBLG186.

$\dot{\gamma}_0/s^{-1}$	$\lambda_{\parallel}^{*}$(ss)/mm	$\lambda_{\perp}^{*}$(ss)/mm	$\sqrt{\dot{\gamma}_0}\lambda_{\parallel}^{*}$(ss)/mms$^{-1/2}$	$\sqrt{\dot{\gamma}}\lambda_{\perp}^{*}$(ss)/mms$^{-1/2}$	t_b/s
2·57	0·041	0·015	0·065	0·024	33
5·14	0·030	0·010	0·070	0·023	20
10·28	0·033	0·011	0·11	0·035	8
20·57	0·029	0·0099	0·13	0·045	3

approach. Table 2 shows that the time t_b for band formation is roughly inversely proportional to the prior shear rate.

As noted above, $\lambda_{\parallel}^{*} > \lambda_{\perp}^{*}$ immediately after cessation of shearing. Consistent with this observation, table 2 shows that $\lambda_{\parallel}^{*}(ss) > \lambda_{\perp}^{*}(ss)$ during shearing. Here ss denotes a steady state value during shear. This result, $\lambda_{\parallel}^{*}(ss) > \lambda_{\perp}^{*}(ss)$, is consistent with the appearance of stripes parallel to the flow direction during shearing. Note that both $\lambda_{\parallel}^{*}(ss)$ and $\lambda_{\perp}^{*}(ss)$ are weakly decreasing functions of $\dot{\gamma}_0$.

Figure 10 shows $\lambda_{\parallel}^{*}$ versus time for a series of shear rates, again for PBLG186 at a gap h of 175 μm. For each shear rate greater than $2{\cdot}57\,s^{-1}$, the growth of the band spacing is similar: $\lambda_{\parallel}^{*}$ is initially around 30 or 40 μm, and grows to about 80 μm within about 100 s. Even the results for $\dot{\gamma}_0 = 2{\cdot}57\,s^{-1}$ during the period in which bands exist falls more or less on the same curve as the other shear rates. The departure of the results for $\dot{\gamma}_0 = 2{\cdot}57\,s^{-1}$ from the other curves exists only at short times where the bands were not visible for this shear rate.

Figure 11 shows $\lambda_{\perp}^{*}$ versus time for the same runs as in figure 10. In contrast to figure 10, the rise in $\lambda_{\perp}^{*}$ with time becomes much steeper as $\dot{\gamma}_0$ increases, and the curves are nowhere close to superimposing. We believe that the steepening rise in $\lambda_{\perp}^{*}$ as the shear rate increases reflects the increasing speed of band formation.

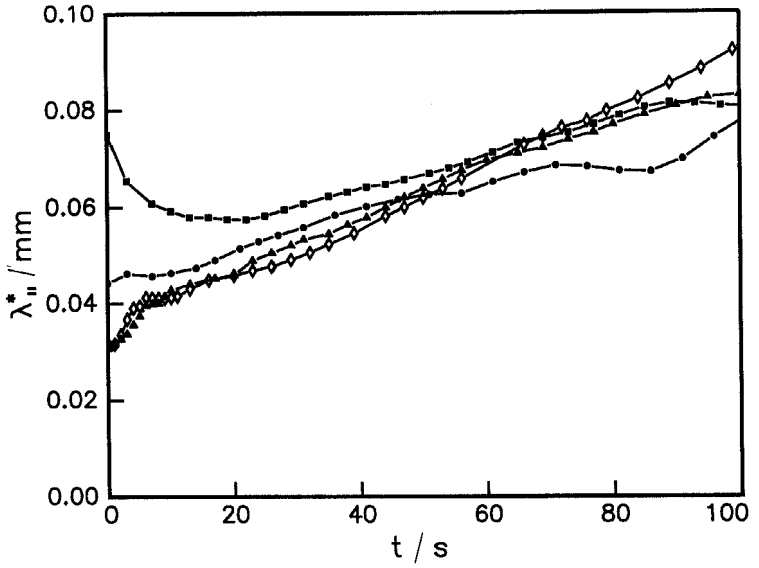

Figure 10. $\lambda^*_{\parallel}$ versus time for PBLG186 at four different shear rates (■, 2·57 s^{-1}; ●, 5·14 s^{-1}; ▲, 10·28 s^{-1}; ◇, 20·57 s^{-1}); $h = 175\,\mu m$, $\gamma_0 \approx 1400$.

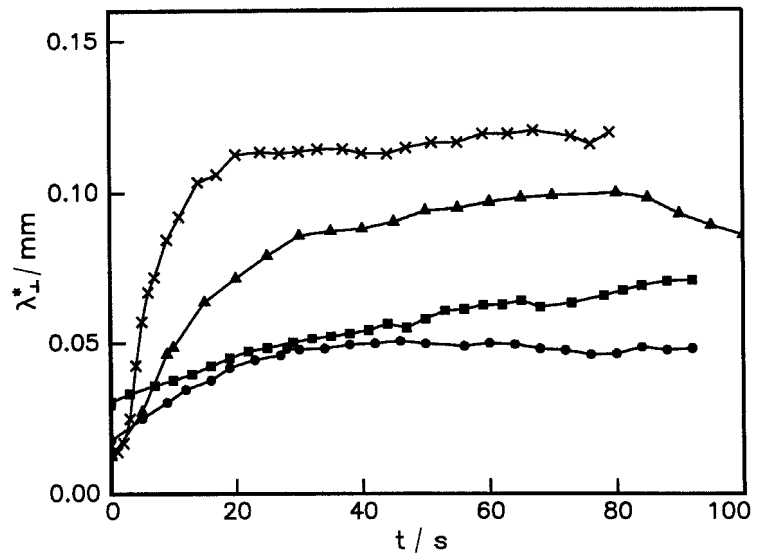

Figure 11. $\lambda^*_{\perp}$ versus time for PBLG186 at four different shear rates (■, 2·56 s^{-1}; ●, 5·12 s^{-1}; ▲, 10·28 s^{-1}; ×, 20·56 s^{-1}); $h = 175\,\mu m$, $\gamma_0 \approx 1400$; same runs as figure 11.

Kiss and Porter [16] noted that 'with increasing rate of prior shear the [banded] texture forms more rapidly, with... thinner striations'. Our studies are consistent with Kiss and Porter, in that the initial band spacing decreases slightly with increased shear rate; however, once the bands form they have the same spacing no matter what the shear rate is, if the comparison is made at the same time after cessation of shearing. This seemingly contradictory result is possible, because the bands form more quickly, and are initially thinner, at higher shear rates.

We should note that the value $\lambda_{\|}^{*}$ we report here is not exactly the same as the band width reported by some others in visual observations. First, our $\lambda_{\|}^{*}$ is a periodicity length, and thus would encompass one repeat period, that is the width of a light band combined with its neighbouring dark zone. Most reports of the band width seem to refer to the width of the light band only. Because of this factor alone, our $\lambda_{\|}^{*}$ values will be larger than the band widths reported by others. Also, our $\lambda_{\|}^{*}$ is a characteristic wavelength, and subsequently the long wavelength irregularities or modulations in light intensity that we typically see superimposed on the band structure serve to increase somewhat further our $\lambda_{\|}^{*}$ values. Hence the band width that we might measure from images such as figures 5 and 6 are perhaps about one third the value of $\lambda_{\|}^{*}$ obtained from the Fourier spectrum. Thus, figure 10 is consistent with the conclusion drawn from a study carried out in parallel with ours, that for PBLG solutions the visually observed band width grows from about 10 μm to 30 μm within 100 s after shearing ceases [35].

For the PBG solutions of table 1, at times 100 s or more after cessation of shearing, and for shear rates greater than about 20 s^{-1}, the reproducibility of our plots of $\lambda_{\|}^{*}$ versus time is poor; hence the results in figures 8–11 were restricted to the range shown. We did repeatedly note, however, that at long times ($t > 100$ s) $\lambda_{\|}^{*}$ goes through a maximum at a value of $\lambda_{\|}^{*}$ roughly equal to the gap h. At shorter times ($t < 100$ s) we find little gap dependence of $\lambda_{\|}^{*}$, except for cases in which h is small enough to be comparable to the initial value of $\lambda_{\|}^{*}$.

Figure 12 contains the image and the horizontal FFT for a case in which the shear rate is low enough ($\dot{\gamma} = 3{\cdot}6\ s^{-1}$ and $h = 250\ \mu$m, for PBG118) such that bands do not appear. The Fourier spectrum still shows a broad response, although it is not as flat as before. Based on a comparison of the spectra in figures 4(*b*) and 12 alone, it would be difficult to say in which case bands appear. We have noted, however, a dynamical signature of the banded structure. In the case where bands do not appear, $\lambda_{\|}^{*}$ is always observed to decrease with time, in contrast to when bands form; this is shown in figure 13. We believe that this decrease in $\lambda_{\|}^{*}$ with time is caused by the disappearance, after cessation of shearing, of the striped texture parallel to flow. When bands form, but only slowly, as they do for $\dot{\gamma}_0 = 2{\cdot}57\ s^{-1}$, $\lambda_{\|}^{*}$ often initially decreases with time, followed by an eventual increase (see figure 10).

Figure 14 shows $\lambda_{\|}^{*}$ versus time for PBLG238, PBLG186, and PBG118 at a shear rate of about 10 s^{-1}. The viscosities of these three samples range from a low of 4 P for PBG118 to a high of 100 P for PBLG238. The results are roughly similar for all three; that is, $\lambda_{\|}^{*}$ lies in the range 30–80 μm and generally increases with time. For the lowest viscosity material, PBG118, the shear rate of 10 s^{-1} is only a factor of two above the minimum required to form bands, and we see that $\lambda_{\|}^{*}$ at first decreases with time. This decrease followed by an increase in $\lambda_{\|}^{*}$ seems to be an intermediate response between that for low Deborah numbers, where only a decrease occurs (see figure 12), and the response for modest or high Deborah numbers, where only the increase is seen.

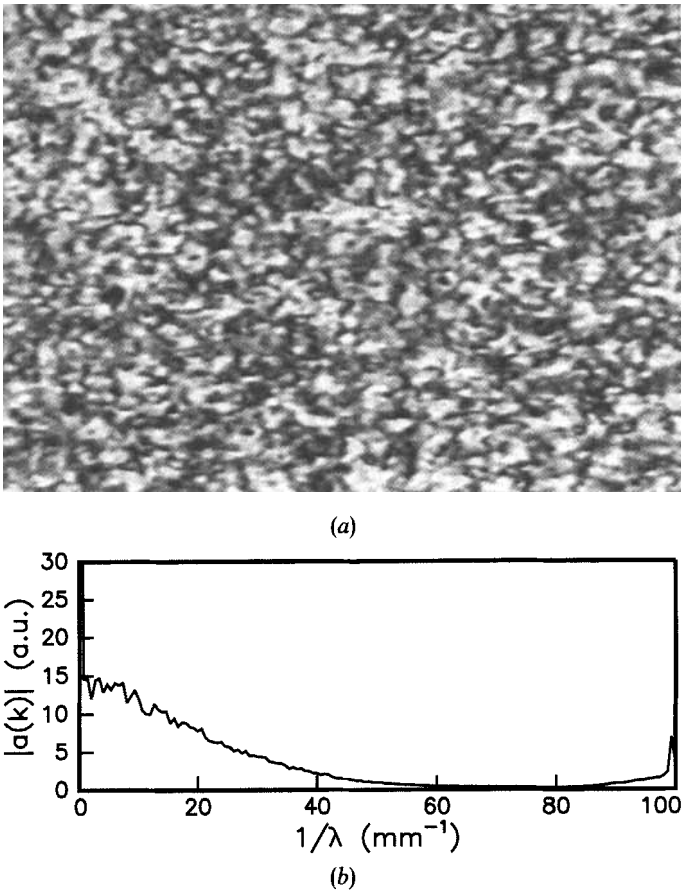

Figure 12. (*a*) Image of texture of PBG118 90 s after shear stopped; bands do not form in this case. $\dot{\gamma}_0 = 3{\cdot}6\,s^{-1}$, $\gamma_0 = 972$, $h = 250\,\mu m$. The horizontal width of the image is about $1500\,\mu m$. (*b*) FFT obtained from the image in (*a*).

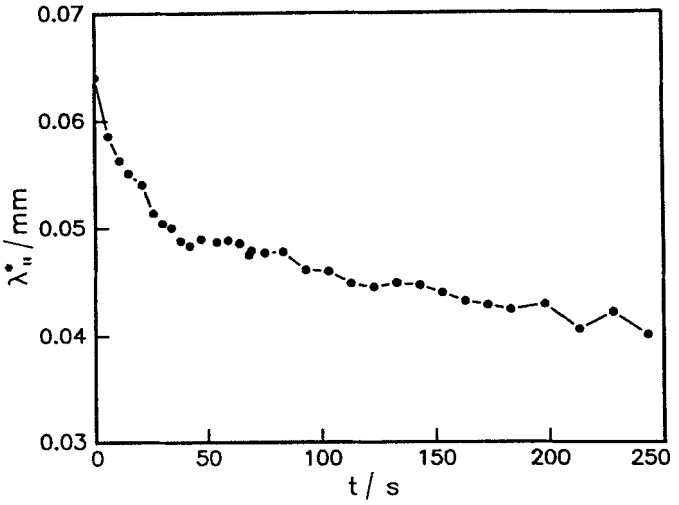

Figure 13. $\lambda_{\parallel}^{*}$ versus time for the case in the previous figure where bands were not observed. Note the monotonic decrease of $\lambda_{\parallel}^{*}$ with time.

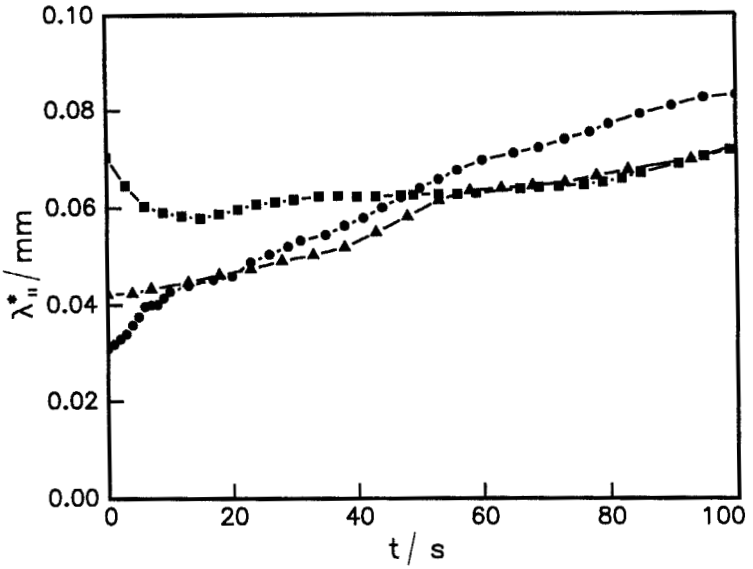

Figure 14. $\lambda^*_{\parallel}$ versus time for PBLG238 (▲, MW = 238 000), PBLG186 (●, MW = 186 000), and PBG118 (■, MW = 118 000) at a shear rate $\dot{\gamma}_0$ of approximately $10\,s^{-1}$. For PBLG186 and PBG118, $h = 175\,\mu m$, while for PBLG238, $h \approx 50\,\mu m$. In each case the shear strain γ_0 is 1000 or more.

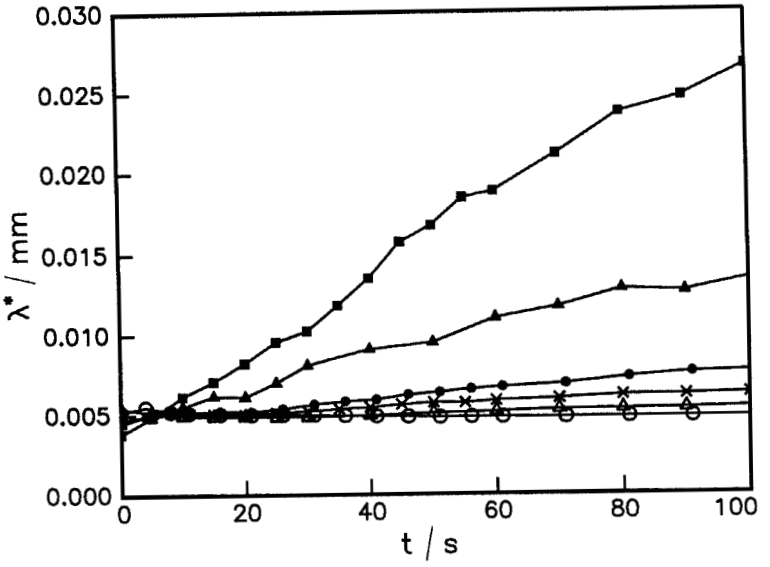

Figure 15. $\lambda^*_{\parallel}$ (○, $1{\cdot}2\,s^{-1}$; △, $2{\cdot}4\,s^{-1}$; ×, $6{\cdot}0\,s^{-1}$) and $\lambda^*_{\perp}$ (●, $1{\cdot}2\,s^{-1}$; ▲, $2{\cdot}4\,s^{-1}$; ■, $6{\cdot}0\,s^{-1}$) versus time for a solution of HPC (Klucel L) with $\dot{\gamma}_0 \approx 1{\cdot}5\,s^{-1}$, $2{\cdot}4\,s^{-1}$, and $6\,s^{-1}$, $\gamma_0 \approx 200$, and $h \approx 50\,\mu m$. The bands can be seen by eye at $t \approx 85\,s$, 40 s, and 30 s when $\dot{\gamma}_0 \approx 1{\cdot}5\,s^{-1}$, $2{\cdot}4\,s^{-1}$ and $6\,s^{-1}$, respectively.

We also analysed the development of banded textures in a viscous HPC solution over a limited range of conditions. For this solution, the bands were so fine that they could not easily be resolved with the objective $\times 10$ magnification. Hence they were videotaped through a combination of a $\times 20$ magnification objective and a $\times 5$ magnification eyepiece, for a total magnification of $\times 100$. Figure 15 shows results for $\lambda_{\parallel}^{*}(t)$ and $\lambda_{\perp}^{*}(t)$ at shear rates $\dot{\gamma}_0 \approx 1{\cdot}5, 2{\cdot}4$, and $6\,s^{-1}$ and at a gap h of roughly 50 μm. For the HPC solution, as for the PBG solutions, bands form more quickly as $\dot{\gamma}_0$ is increased, and $\lambda_{\perp}^{*}(t)$ (closed symbols) grows more rapidly as $\dot{\gamma}_0$ increases, while $\lambda_{\parallel}^{*}(t)$ is nearly independent of $\dot{\gamma}_0$. The results for the HPC solution differ from those for low viscosity PBG solutions, however, in that the bands in HPC are five times finer than the initial band spacing for the PBG solutions and they grow with time much more slowly, so that no change is seen within approximately the first 300 s after shearing ceases. These results for HPC are consistent with those of Fincher, who also found b to be independent of both $\dot{\gamma}_0$ and t. In the HPC solution, the absence of an observable increase in $\lambda_{\parallel}^{*}$ within the first 300 s is perhaps not surprising, since the viscosity of this solution at low shear rates ($<1\,s^{-1}$) is very high: being greater than 3000 P.

4. Energy sources for band formation

While the precise mechanism of band formation is still uncertain [18, 22, 24, 26] there are only two possible sources of elastic energy that could drive the phenomenon. The first is molecular elasticity, already mentioned in § 2.1; the second is texture elasticity. As stated previously, molecular elasticity is the energy stored in distortion of the local molecular order parameter from its equilibrium value. This molecular distortion occurs when velocity gradients are high enough that the degree of orientational order is made either higher or lower than it would be at equilibrium; the distortion becomes significant when the Deborah number becomes appreciable. The Deborah number De is defined as

$$De \equiv \dot{\gamma}_0 \tau_{mol}, \tag{2}$$

where τ_{mol} is a characteristic molecular relaxation time.

The second source of elastic energy that might drive band formation is the elasticity stored in the texture, i.e. the micron-scale orientational inhomogeneities created or amplified by the previous shearing flow [6, 36]. Like molecular elasticity, the influence of texture elasticity in the flow can be quantified by a dimensionless number, in this case an Ericksen number

$$Er \equiv \dot{\gamma}_0 \tau_{tex}, \tag{3}$$

where τ_{tex} is the texture relaxation time given by

$$\tau_{tex} \propto \frac{\eta}{E_{tex}}, \tag{4}$$

and E_{tex} is the elastic energy density stored in the texture. Thus the Ericksen number is given by

$$Er = \frac{\dot{\gamma}_0 \eta}{E_{tex}}, \tag{5}$$

where now Er is just the ratio of the viscous energy $\dot{\gamma}_0 \eta$ to the texture energy. Under a shearing flow, viscous energy distorts the director field until the texture energy grows to a level sufficient to resist further distortion [6]. Marrrucci [11, 12] has proposed that

the point at which the director distortion comes to a steady state in the shear field is such that the distortion energy E_{tex} is proportional to the viscous energy $\dot{\gamma}_0\eta$. Thus

$$E_{tex} \propto \dot{\gamma}_0 \eta, \tag{6}$$

and hence the ratio $\dot{\gamma}_0\eta/E_{tex}$, which is just Er, is expected to be independent of shear rate [37].

If this hypothesis is correct, then there ought to be a range of shear rates over which the domain size shrinks with increased shear rate in a predictable manner. Specifically, if the shear rate is low enough that the domain size a is much larger than the molecular length, then the texture energy should follow the small distortion theory of Frank [38], Oseen [39], Zochar [40] and Ericksen [41], in which all but the lowest order quadratic terms in the director gradient are neglected, and one obtains the scaling

$$E_{tex} \approx \frac{K}{a^2}. \tag{7}$$

Here K is a characteristic Frank elastic constant, which for polymeric nematics has typically a value of about 10^{-6} dyn. [42]. From equations (5) and (7), and the hypothesis that Er is a constant, we find the scaling [11, 12]

$$a \propto \sqrt{\left(\frac{K}{\eta\dot{\gamma}_0}\right)}. \tag{8}$$

Of course, the scaling fails at very low shear rates if a grows to a size comparable to the gap spacing h. Consistent with equation (8), a refinement of the texture, i.e. a decrease in a, has been observed with increasing shear rate $\dot{\gamma}_0$ by Alderman and Mackley [6] on thermotropic liquid-crystalline polymers.

The direct energy source for band formation is almost certainly texture elasticity. This conclusion rests on the observation that molecular elasticity relaxes quickly, in a time τ_{mol}, which for PBLG186 is about 0·03 s. We observed for this fluid, that at low shear rates, the bands required as long as 4 min to form after cessation of shearing. At such long times compared to τ_{mol}, there is virtually no residual molecular elasticity available to drive band formation. The texture relaxation time τ_{tex}, on the other hand, can be long enough to drive band formation many minutes after shearing ceases.

While molecular elasticity is not likely to be the immediate or direct cause of band formation, it is probably an indirect cause, because table 1 shows that there is a threshold Deborah number below which bands do not form. For PBLG86, even after application of more than 1400 strain units, bands did not form at shear rates of less than about 40 s^{-1} or so, while for PBLG186, $\dot{\gamma}_0 \approx 0{\cdot}25\ s^{-1}$ was sufficient to form bands. This variation in the critical shear rate for band formation correlates with the shear rate $\dot{\gamma}_{me}$ at which the first normal stress difference passes through its first positive maximum. For the four materials in table 1 for which $\dot{\gamma}_b$ was determined, the ratio $\dot{\gamma}_b/\dot{\gamma}_{me}$ falls in the range $\approx 0{\cdot}02$–$0{\cdot}07$. Thus, in these solutions of widely differing viscosity and relaxation time, there seems to be a critical Deborah number, $De_c \approx 0{\cdot}01$–$0{\cdot}04$ for band formation (based on the observation made earlier that $De \approx 0{\cdot}5$ when $\dot{\gamma}_0 = \dot{\gamma}_{me}$). Thus, molecular elastic effects during shearing seem to be necessary to produce the texture that in turn drives band formation after shearing ceases. As the imposed strain is increased, the required level of molecular elasticity (and hence the magnitude of the required Deborah number) decreases, possibly to some limiting value. Thus a complete explanation of band formation probably involves both texture elasticity and molecular elasticity.

If, as we have suggested, texture elasticity is the energy source directly responsible for band formation, we might expect the time required to form bands, and the initial band spacing, to follow a scaling with shear rate given by a balance of the texture elastic energy that drives band formation against the resisting viscous force. This balance gives for the time t_b for bands to form:

$$t_b \approx \frac{\eta}{E_{tex}} \approx \frac{1}{\dot{\gamma}_0}, \tag{9}$$

where we have used equation (6). Thus t_b should decrease as $\dot{\gamma}_0$ increases as $\dot{\gamma}_0^{-1}$; this is roughly what we and others [16, 24, 29] have seen (see table 2).

Likewise, if this argument is correct, and if we can assume that the texture energy is given by the Frank theory, then the band spacing b should be controlled by the continuum quantities η, K, $\dot{\gamma}_0$, and t. The only independent dimensionless quantities that can be formed from these and the band spacing b are

$$b(\eta\dot{\gamma}_0/K)^{1/2}; \quad t\dot{\gamma}_0. \tag{10}$$

From this, we conclude that b should decrease with increased viscosity η or shear rate $\dot{\gamma}_0$ as $(\dot{\gamma}_0\eta)^{-1/2}$. However, we have found for the PBG solutions of table 1 that there is little change in $\lambda_{\parallel}^{*}$ when $\dot{\gamma}_0$ is changed by a factor of 10 or η is changed by factor of 25 (see figures 10 and 14). The failure of the scaling implicit in equation (10) is shown in figure 16, which is a plot of $\lambda_{\parallel}^{*}(\dot{\gamma}_0)^{1/2}$ versus $t\dot{\gamma}_0$ for various shear rates with a single material (and hence fixed values of K and η). This plot does not collapse the data. A much more nearly universal curve is obtained merely by plotting $\lambda_{\parallel}^{*}$ versus t (see figure 10). Note also in table 2 that the stripe spacing during shear, $\lambda_{\perp}^{*}(\text{ss})$, does not seem to scale as $\dot{\gamma}_0^{-1/2}$. Instead, $\lambda_{\parallel}^{*}(\text{ss})$ and $\lambda_{\perp}^{*}(\text{ss})$, as well as $\lambda_{\parallel}^{*}(t)$ for small t (see figure 10) seems to show a weaker dependence on $\dot{\gamma}_0$ than $\dot{\gamma}_0^{-1/2}$. Thus the scaling for the band spacing b that we predict from the small gradient (or Frank) theory of texture elasticity is not satisfied.

One possible explanation for this failure of the scaling law is that under conditions necessary for band formation, the texture during shear is too fine for Frank theory to be valid. While the band wavelength is certainly wide enough ($> 20\,\mu$m) to be described by Frank theory, the striped texture, which is the precursor to the bands, is characterized by a very broad distribution of wavelengths, centred at about $10\,\mu$m, but extending down at least to a few micrometres. Furthermore, the finest texture length scales in a tumbling nematic or cholesteric are probably those in the z (gap) direction, which are not observable in our experiments. Hence, it is plausible that the smallest texture length scales are actually of the order of a micrometer or even less, close enough to the molecular persistence length scale ($0{\cdot}1\,\mu$m for our PBGs) for the Frank theory to fail.

The existence of a fine scale in the z direction can be inferred indirectly from the observable texture coarsening process in the xy plane. Figures 10 and 11 show that as the shear rate increases, in the y direction both the texture length scale and its rate of growth increase, while there is scarcely any change in the x direction. Thus the texture in the xy plane is both coarser and coarsening faster at high $\dot{\gamma}_0$ than at low $\dot{\gamma}_0$. But if texture energy drives the coarsening process, and this energy is weaker for coarser textures, then the fine texture necessary to drive the rapid coarsening at high $\dot{\gamma}_0$ must reside in the z direction.

If, indeed, the textures of sheared liquid-crystalline polymers become so fine that the Frank theory fails, it is plausible that higher order gradient terms would cause the texture refinement to saturate at a length scale that is several multiples of the molecular

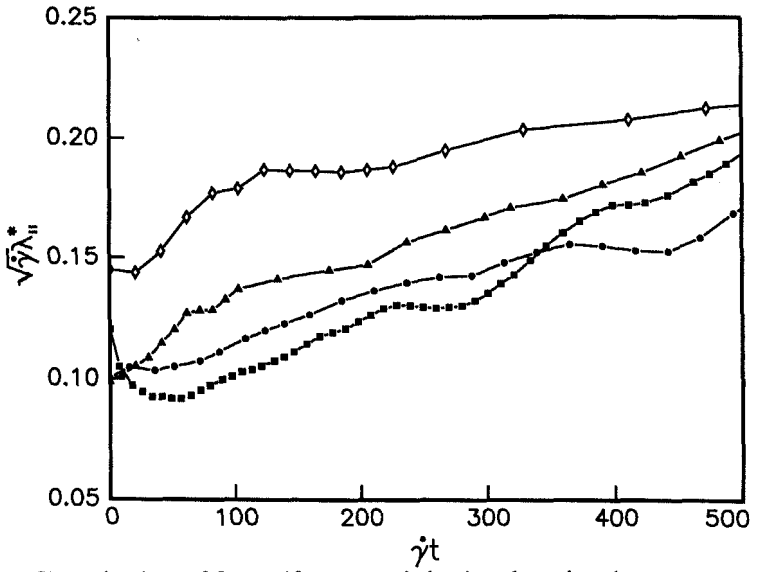

Figure 16. Here the data of figure 10 are rescaled using the prior shear rate $\dot{\gamma}_0$ to check the assumption that the time and shear rate dependences of $\lambda_{\parallel}^{*}$ are controlled by the small-gradient Frank elasticity according to equation (10). ■, $2{\cdot}57\,s^{-1}$; ●, $5{\cdot}14\,s^{-1}$; ▲, $10{\cdot}28\,s^{-1}$; ◇, $20{\cdot}57\,s^{-1}$.

length for a stiff molecule or of the persistence length for a semi-flexible molecule. This might explain the very weak decrease in the texture length scales with increased shear rate (see table 2) or viscosity. It may be more than coincidental that the initial band spacing in PBG solutions is roughly 5–10 times larger than in HPC solutions, while the persistence length of PBG [43] is also 5–10 times larger than that of HPC [44].

If the texture length scale saturates at a scale set by a molecular length or a persistence length, the texture energy E_{tex} does not necessarily saturate, but might continue to rise in proportion to $\dot{\gamma}_0\eta$, as long as there are higher order terms in the gradient expansion capable of providing the increased texture energy. In this way, the observed scaling of t_b with $\dot{\gamma}_0^{-1}$ (see table 2) might be reconciled with our failure to observe the length scaling $b \propto (\dot{\gamma}_0\eta)^{-1/2}$ predicted using the Frank form of texture elasticity.

Of course, if the shear rate is reduced enough, the texture should be describable using Frank theory. But evidently because there is a minimum Deborah number for band formation, for our solutions Frank theory fails at all shear rates high enough to form bands. We might think that by making the molecular weight high enough, the critical shear rate for band formation could be made low enough for Frank theory to hold. But as the molecular weight increases, so does the viscosity, and this increases the shear stress. If, as seems likely, Frank theory fails at a critical value of the shear stress, then it may be difficult to find a polymeric liquid crystal which still satisfies Frank theory at shear rates high enough for bands to form.

5. Summary

We have used video image analysis to quantify the development of bands transverse to the shear direction after cessation of shearing. We find that the widening of the bands observed by ourselves and others in PBG solutions occurs via a disappearance of short wavelength structures and an enhancement of the intensity associated with longer

wavelengths. We also find in PBG solutions that at long times (>100 s) after shearing ceases, the characteristic wavelength $\lambda_{\parallel}^{*}$ often goes through a maximum value equal to or slightly less in magnitude than the gap h.

The time to form bands t_b roughly obeys the scaling with shear rate, $t_b \propto \dot{\gamma}_0^{-1}$, expected from the assumption that the texture energy density E_{tex} increases in proportion to $\dot{\gamma}_0\eta$. However, our failure to observe more than a very weak dependence of band spacing on $\dot{\gamma}_0$ or η indicates that at shear rates high enough to form bands, the texture energy density is too high to be described by the Frank theory, which would give $b \propto (\dot{\gamma}_0\eta)^{-1/2}$. Indeed, a comparison of the band spacing for PBG and HPC indicates that the texture length scale saturates at a fine scale proportional to the persistence length of the molecule.

A role for molecular elasticity in the formation of bands is shown in our observation that a value of the Deborah number *De* of about 0·01–0·04 seems necessary for band formation; as *De* is lowered to this minimum value, the amount of strain required to form bands diverges. Yet just above this minimum *De*, the time required for bands to form after shearing ceases becomes so long that molecular elasticity can have no direct role in the process. We conclude, therefore, that the role of molecular elasticity ends when shear ceases; but during shear, molecular elasticity helps to produce a texture that can drive band formation after shearing ceases. If *De* is near its minimum value for band formation, then the shearing must persist for hundreds of strain units for the cumulative effects of molecular elasticity to induce the needed texture.

J. T. Gleeson acknowledges support from the Natural Sciences and Engineering Research Council of Canada. We thank Jan Mewis and Paula Moldenaers with whom R. G. Larson had useful discussions.

References

[1] Fernandes, J. R., and DuPre, D. B., 1981, *Molec. Crystals liq. Crystals*, **72,** 67.
[2] Taratuta, V. G., Srajer, G. M., and Meyer, R. B., 1985, *Molec. Crystals liq. Crystals*, **116,** 245.
[3] Srinivasarao, M., and Berry, G. C., 1990, *J. Rheol.*, **35,** 379.
[4] Burghardt, W. R., and Fuller, G. G., 1990, *Macromolecules*, **24,** 2546.
[5] Mackley, M. R., Pinaud, F., and Siekmann, G., 1981, *Polymer*, **22,** 437.
[6] Alderman, N. J., and Mackley, M. R., 1985, *Faraday Discuss. chem. Soc.*, **79,** paper 12.
[7] Moldenaers, P., Yanase, H., and Mewis, J., 1990, *ACS Symposium Series*, **435,** 370.
[8] Moldenaers, P., Fuller, G. G., and Mewis, J., 1989, *Macromolecules*, **22,** 960.
[9] Moldenaers, P., and Mewis, J., 1986, *J. Rheol.*, **30,** 567.
[10] Larson, R. G., and Mead, D. W., 1989, *J. Rheol.*, **33,** 185.
[11] Marrucci, G., 1985, *Pure appl. Chem.*, **57,** 1545.
[12] Marrucci, G., 1984, *Proceedings of the 9th International Congress on Rheology*, Acapulco, Mexico 8th October to 13th.
[13] Wissbrun, K., 1985, *Faraday Discuss. chem. Soc.*, **79,** 161.
[14] Marrucci, G., and Maffetone, P. L., 1990, *J. Rheol.*, **34,** 1217, 1231; 1991, *Ibid.*, **35,** 313 (erratum).
[15] Larson, R. G., and Doi, M., 1990, *J. Rheol.*, **35,** 539.
[16] Kiss, G., and Porter, R. S., 1980, *Molec. Crystals liq. Crystals*, **60,** 267.
[17] Zachariades, A. E., and Logan, J. P., 1983, *Polym. Engng. Sci.*, **23,** 797.
[18] Zachariades, A. E., Navard, P., and Logan, J. P., 1984, *Molec. Crystals liq. Crystals*, **110,** 93.
[19] Navard, P., and Zachariades, A. E., 1987, *J. Polym. Sci. Polym. Phys.*, **25,** 1089.
[20] Takeuchi, Y., Shuto, Y., and Yamamoto, F., 1988, *Polymer*, **29,** 605.
[21] Viney, C., and Windle, A. H., 1987, *Phil. Mag.* A, **55,** 463.
[22] Nishio, Y., Yamane, T., and Takahashi, T., 1985, *J. Polym. Sci. Polym. Phys.*, **23,** 1053.

[23] NAVARD, P., 1986, *J. Polym. Sci. Polym. Phys.*, **24,** 435.
[24] ERNST, B., and NAVARD, P., 1989, *Macromolecules*, **22,** 1419.
[25] MARRUCCI, G., GRIZZUTI, N., BUONAURIO, A., 1987, *Molec. Crystals liq. Crystals*, **153,** 263.
[26] MAFFETTONE, P. L., GRIZZUTI, N., and MARRUCCI, G., 1989, *Liq. Crystals*, **4,** 385.
[27] FRIED, F., and SIXOU, P., 1988, *Molec. Crystals liq. Crystals* B, **158,** 163.
[28] FINCHER, C. R., JR., *Molec. Crystals liq. Crystals*, **155,** 559.
[29] MARSANO, E., CARPANETO, L., CIFERRI, A., and WU, Y., 1988, *Liq. Crystals*, **3,** 1561.
[30] KISS, G., and PORTER, R. S., 1978, *J. Polym. Sci. Polym. Symp.*, **65,** 193.
[31] MOLDENAERS, P., and MEWIS, J., 1986, *J. Rheol.*, **30,** 567.
[32] DOI, M., 1980, *Ferroelectrics*, **30,** 247; DOI, M., and EDWARDS, S. F., 1986, *The Theory of Polymer Dynamics* (Oxford Press).
[33] MARRUCCI, G., and MAFFETTONE, P. L., 1989, *Macromolecules*, **22,** 4076.
[34] LARSON, R. G., 1990, *Macromolecules*, **23,** 3983.
[35] MOLDENAERS, P., and MEWIS, J. (to be published).
[36] ONOGI, S., and ASADA, T., 1980, *Rheology*, Vol. 1, edited by G. Astarita, G. Marrucci and L. Nicolais (Plenum Press).
[37] BURGHARDT, W. R., and FULLER, G. G., 1990, *J. Rheol.*, **34,** 959.
[38] FRANK, F. C., 1958, *Discuss. Faraday Soc.*, **25,** 19.
[39] OSEEN, C. W., 1983, *Trans. Faraday Soc.*, **29,** 883.
[40] ZOCHER, H., 1933, *Trans. Faraday Soc.*, **29,** 945.
[41] ERICKSEN, J. L., 1966, *Archs ration. Mech. Analysis*, **23,** 266.
[42] LEE, S.-D., and MEYER, R. B., 1988, *Phys. Rev. Lett.*, **61,** 2217.
[43] PARATHASARATHY, R., HOUPT, D. J., and DUPRE, D. B., 1988, *Liq. Crystals*, **3,** 1073.
[44] SHTENNIKOVA, I. N., KOLBINA, G. F., SHBAEV, V. P., and EKAEVA, I. V., 1990, *Eur. Polym. J.*, **26,** 787.